# Mapping yeast mitotic 5' resection at base resolution

# reveals the sequence and positional dependence of nucleases *in vivo*

Dominic Bazzano[1,2], Stephanie Lomonaco[1], Thomas E. Wilson[1,2,*]

[1] Department of Pathology
[2] Department of Human Genetics
University of Michigan, Ann Arbor, 48109

[*] Corresponding Author
2065 BSRB
109 Zina Pitcher Place
University of Michigan
Ann Arbor MI, 48109-2200
Phone: 734-764-2212
wilsonte@umich.edu

Keywords: DNA repair, double strand break, resection, recombination, mitotic

**Abstract**

Resection of the 5'-terminated strand at DNA double strand breaks (DSBs) is the critical regulated step in the transition to homologous recombination. Biochemical and genetic studies have led to a multi-step model of DSB resection in which endonucleolytic cleavage mediated by Mre11 in partnership with Sae2 is coupled with exonucleolytic cleavage mediated by redundant pathways catalyzed by Exo1 and Sgs1/Dna2. These models have not been well tested at mitotic DSBs *in vivo* because most methods commonly used to monitor resection cannot precisely map early cleavage events. Here we report resection monitoring with next-generation sequencing in which unique molecular identifiers allow exact counting of cleaved 5' ends at base pair resolution. Mutant strains, including *exo1*Δ, *mre11*-H125N, *exo1*Δ and *exo1*Δ *sgs1*Δ, revealed a major Mre11-dependent cleavage position 60 to 70 bp from the DSB end whose exact position depended on local sequence and tracked an apparent motif. They further revealed an Exo1-dependent pause point approximately 200 bp from the DSB. Suppressing resection extension in *exo1*Δ *sgs1*Δ yeast exposed a footprint of regions where cleavage was restricted within 119 bp of the DSB and near the Exo1 pause point and where it was much less restrained. These results provide detailed *in vivo* support of prevailing models of DSB resection and extend them to show the combined influence of sequence specificity and access restrictions on Mre11 and Exo1 nucleases.

## Introduction

Accurate and efficient repair of DNA double-strand breaks (DSBs) is critical to cell survival and proper genomic function (1). These cytotoxic DNA lesions arise due to exogenous and endogenous agents, such as radiation and impaired cellular replication (2). In addition, DSBs can arise from regulated physiological reactions such as yeast mating type switching and V(D)J recombination in developing lymphocytes (3, 4).

Two evolutionarily conserved pathways exist to repair DSBs: non-homologous end joining (NHEJ) and homologous recombination (HR) (5, 6). In NHEJ, DSB termini are rapidly bound by the Ku heterodimer, a clamp-like protein complex comprised of Yku70 and Yku80 in yeast (7). Ku binding constrains nuclease activity at DSB ends and promotes the association of downstream proteins critical to repair (8). The Mre11-Rad50-Xrs2 (MRX) complex also appears at DSBs nearly instantaneously and further promotes downstream signaling, such as Tel1-mediated checkpoint activation (9, 10). MRX also has functions in tethering the two DSB termini and end processing during NHEJ (11, 12). In NHEJ, the two DSB ends are ultimately ligated by DNA Ligase IV (Dnl4 in yeast) (13, 14).

Unlike NHEJ, HR relies on nucleolytic processing of DSB 5'-terminated strands in a process called end resection to create an exposed 3'-terminated strand suitable for donor pairing and extension (15). End resection is proposed to begin through a targeted endonucleolytic incision by Mre11 <100 bp away from the DSB end in a reaction that in yeast is dependent on Rad50 and Sae2 (12, 16). After this incision, Mre11 uses its 3'-5' exonucleolytic activity to degrade DNA back towards the DSB end, destabilizing Ku (17). Long range resection in the 5'-3' direction occurs through Mre11-mediated recruitment of the exonuclease Exo1 or the helicase Sgs1 in partnership with the endonuclease Dna2 (18, 19). The combined activities of Mre11

backtracking towards the DSB end and Exo1- or Sgs1-Dna2-mediated degradation of DNA away from the break comprises the prevailing bidirectional model of resection (20). The resulting ssDNA is ultimately coated by Rad51 to promote HR (21).

While many proteins involved in HR and resection have been identified, there is still much to be learned about the precise coordination of the earliest initiating events as they occur *in vivo*. Prior *in vitro* studies on which current models are based analyzed Mre11 nuclease activity on Ku-occluded synthetic dsDNA ends and characterized a primary incision ~35 bp from the terminus on a 70 bp DNA substrate (22). Wang *et al.* also observed a second incision occurring further downstream at 65 bp from the DNA end in addition to the 35 bp incision when the DNA substrate length was increased to 100 bp (23). Such work led to a hypothesis that Mre11 makes stepwise endonucleolytic incisions from DSB termini to initiate resection (24).

Evidence directly supporting such highly precise models of resection is lacking for mitotic DSBs *in vivo*. Most current methods used to monitor resection in *in vivo* typically use qPCR- or Southern Blot-based approaches to quantify ssDNA appearance beginning 100s of bp from the DSB end (25, 26), outside of the window examined by *in vitro* studies. These methods are highly informative regarding resection kinetics but lack the resolution needed to understand the exact sequence of events during resection initiation, specifically with regard to Mre11 and Exo1 nuclease activity and the factors that promote or constrain their patterns of action. The covalent linkage of Spo11 to meiotic DSB 5' termini has permitted more detailed pictures but these advantages are not available for mitotic DSBs (27).

We developed a novel *in vivo* resection assay to map mitotic end resection at a site-specific DSB in budding yeast at base-pair resolution. High molecular weight DNA was subjected to primer extension and ligation into circles in a manner that allowed exact counts of

the molecules terminated at all possible resection positions within ~350 bp of the DSB. Loss of Exo1 resulted in increased signal throughout that window, most notably at a position -65/-66 bp from the DSB end that proved to be Mre11-dependent, in explicit support of prevailing resection models (23). This pattern was not rigidly positioned but instead moved at different DSB ends in a manner that suggested a sequence motif preference. A distinct at position -206 bp from the DSB was Exo1-dependent and suggested a pause point in progressive resection. The pattern in *exo1 sgs1* mutant yeast exposed a "footprint" of factors restricting cleavage activity near the DSB. Other mutants revealed dynamic activities at the extreme DSB terminus. These studies provide a precise view of the nuclease activities at DSB ends in living mitotic cells and of the sequence-and position-dependent factors that constrain them.

## Results

### Mapping end resection intermediates in NHEJ-deficient yeast

The DSB system was previously described (28) and includes (i) the HO endonuclease coding sequence placed under control of the native *GAL1* promoter and (ii) a single HO cut site (HOcs) in a nucleosome-free region of the *ILV1* promoter. To facilitate resection monitoring without competing NHEJ, we added a *dnl4*-K466A mutation to all strains that renders Dnl4 catalytically inactive but still able to bind normally to DSBs (29), henceforth referred to as wild-type (WT) with respect to DSB resection. These alleles result in rapid and irreversible generation of a site-specific DSB at *IVL1* in >90% of cells within 30 minutes of adding galactose (Figure 1A, Supplementary Figure 1). At 45 minutes after DSB induction, cultures were resuspended in dextrose media to suppress HO expression and stimulate resection (30) as measured in Figure 1B using a ddPCR method based on the resistance of resected ssDNA to digestion by a restriction endonuclease (RE) (26). Great care was taken to extract high molecular weight genomic DNA (gDNA) given that sheared gDNA is indistinguishable from resection intermediates (Supplementary Figure 2).

We further added a control allele to our strains that lacked a DSB but had (i) a shared common sequence with the DSB allele and (ii) a unique sequence abutting an NdeI restriction site, the same site as found 84 bp distal to the *ILV1* HOcs and also within the shared common sequence (Figure 1C, panel 1). Purified gDNA was digested with NdeI followed by annealing and extension of a primer that matched the NdeI site in the shared common sequence, which incorporated a randomized 12 bp unique molecular identifier (UMI) and a time point barcode into each gDNA molecule (Figure 1C, panel 2). Intramolecular ligation created a covalent bond between the UMIs and the 5’ ends of both DSB and control DNA molecules, which might have

been created by NdeI, HO, 5’ resection or random shearing (Figure 1C, panel 3). PCR amplification of pooled ligation products to minimize batch effects added P5 and P7 sequences for high throughput sequencing (Figure 1D). Because the primer extension primer had a 5’ hydroxyl, only gDNA strands with 5’ phosphates could give final products.

After sequencing, unique source molecules were computationally assigned to the mappable positions of the DSB and control alleles (see Methods). An average of 21M (range 8M to 34M) unique source molecules were obtained per time point (Supplementary File 1). We could not reliably quantify molecules matching the DSB HO and NdeI ends due to UMI saturation but could quantify the control locus because we used a mixture in which only 5% of cells carried the control allele. Both loci had a minimal background signal at internal positions before the DSB was formed (Supplementary Figure 3). At 35 minutes, signal at the DSB allele shifted to the HOcs position, referred to as position 0, and at further time points we observed resection signal above background at positions internal to only the DSB allele (Supplementary Figure 3), referred to with negative numbers that indicate how many bases had been removed from the HO cut end. For visualization, we subtracted the control allele background signal from the DSB allele signal and constructed heat maps (Figure 1E).

**Signal accumulations are evident at distinct positions even in wild-type yeast**

Despite the fact that resection initiation through our ~350 bp measurement window is expected to be efficient in our WT strain, we observed intriguing signal patterns that are explored below. Molecules corresponding to the first few base positions near the HOcs progressively increased from 60 to 90 minutes after DSB induction (Figure 1E-F). Since the DSB had formed by 35 minutes, this increasing signal at 60 minutes must be due to end processing associated with attempted NHEJ or resection initiation. There was also a very specific accumulation of signal

only in the resecting time points at a single -206 position (Figure 1E); the genesis of this peak is addressed below. Finally, when we looked near the -30 and -60 positions suggested as Mre11 cleavage positions by the biochemical experiments of Cejka and Sung, we noted a slight increase in signal at selected positions, especially at -65/-66 (Figure 1E). This signal was weak but compelling due to its location, similar time course as above, and the negative footprint surrounding it where essentially no cleavage was observed (Figure 1G). These results validate the low background of the method and its signal quality.

**Exo1 loss shifts the DSB end resection pattern more than Sgs1 loss**

To add information to the signal patterns above we repeated resection sequencing in strains lacking Exo1 and Sgs1, which are required for the two main long-range resection mechanisms (19, 31). While the *sgs1*Δ resection profile looked largely like that of WT (Figure 2A), *exo1*Δ first led to a decrease in reads aligning near the HOcs, especially at the -2 position, consistent with Exo1 itself being responsible for removing a limited number of terminal bases (Figure 2A-B) (32). In marked contrast, we observed a dramatic increase in reads mapping to the -65/-66 bp position in the absence of Exo1 (Figure 2A,C), indicating that Exo1 did not create this signal but instead was responsible for suppressing it in WT cells. There was minimal signal in *exo1*Δ after the -65/-66 bp position until 119 bp from the DSB, after which there was a steady increase in intermediates throughout the sequencing window. Even with this general increase in reads mapping further away from the DSB termini in *exo1*Δ, loss of Exo1 led to specific loss of the one major peak at the -206 bp position, identifying it as a likely pause point for progressive Exo1-mediated resection (Figure 2A,D). The large difference when comparing *sgs1Δ* and *exo1Δ* resection patterns suggests that Exo1-mediated resection is the preferred mode of end resection initiation near the DSB.

**Mre11 is responsible for the peak at the -65/-66 position**

Results above demonstrate that a protein other than Exo1 must create the signal peak at the -65/-66 position, which prevailing models predict should be Mre11. To explore this, we first examined strains with a complete deletion of *MRE11*. Highly sensitive examination surrounding the -65/-66 position similar to Figure 1G revealed that loss of Mre11 erased the small signal peak observed in WT cells, although intriguingly the negative footprint surrounding that position remained even without Mre11 present (Figure 3A). With the benefit of Mre11 loss we could also discern that less intense signal peaks were present in WT at -42 and -84 (Figure 3A). Here, it is important to note that our method can only map the one 5' terminal position of a source molecule relative to the DSB-distal primer. Thus, we cannot definitively judge how effectively the more DSB-proximal -42 position is cleaved relative to the efficient -65/-66 position, since cleavage at -65/-66 would prevent detection of simultaneous cleavage at -42. We can confidently state that the -65/-66 position is cleaved more efficiently than the -84 position. Importantly, *mre11*Δ also reduced most signal in our interrogation window after the first ~10 bp, including the -206 peak (Figure 3B).

To establish the actions of Mre11 more definitively we added the *mre11*-H125N mutation, which abolishes the Mre11 nuclease activity (33), to our WT and *exo1*Δ strains. The *mre11*-H125N strain by itself behaved very similarly to *mre11*Δ implicating the Mre11 nuclease as being required for the increase in distal resection intermediates (Figure 3A). Examination of *mre11*-H125N *exo1*Δ relative to *exo1*Δ revealed an essentially complete loss of signal at -65/-66, substantially reduced signal at positions -119 and beyond, but in contrast a marked increase in intermediates mapping near the HOcs (Figures 3C,E,F). Sgs1-Dna2 is the primary pathway in the absence of both Mre11 nuclease activity and Exo1 (19). Therefore, the increase in reads near the

DSB end in *mre11*-H125N *exo1*Δ might reflect a shift to resection carried out from the end by Sgs1-Dna2 as opposed to resection beginning from the nick created by Mre11. Intriguingly, analysis of resection kinetics through our sequencing window via the RE-ddPCR assay showed only a small resection defect in a *mre11*-H125N *exo1*Δ double mutant strain compared to *mre11*-H125N and *exo1*Δ single mutants alone (Figure 3B). There is strong evidence that Mre11 has end-chewing activity that aids in Sgs1 loading (34), but the presence of these intermediates in *mre11*-H125N *exo1*Δ indicates that another protein also has such activity. Data obtained from ddPCR resection measurements suggests that Sgs1-Dna2 mediated resection initiation is only slightly less efficient in the absence of Exo1, Mre11 nuclease activity or both.

**Combined loss of Sgs1 and Exo1 reveals the profile of Mre11 activity permissible at a DSB**

It is known that Mre11 is responsible for ~300 bp of resection in *exo1*Δ *sgs1*Δ double mutant yeast defective in long range resection (35). Indeed, ddPCR quantification of ssDNA produced from resection in *exo1*Δ *sgs1*Δ yeast showed a clear decrease in resection efficiency in this strain as compared to WT (Figure 4A). Analysis of *exo1*Δ *sgs1*Δ yeast in our sequencing assay revealed a large increase in signal at similar positions as observed in the single *exo1Δ* mutant strain (Figures 4B,D, note the scale difference in Figure 4D). The only locations where reads were decreased in *exo1*Δ *sgs1*Δ compared to *sgs1*Δ or *exo1*Δ single mutants were at the positions very near to the DSB termini, indicating that end chewing events in resection are dependent on the presence of Sgs1 or Exo1.

Interestingly, the percentage of unique reads at the -65/-66 bp position was only modestly elevated in *exo1*Δ *sgs1*Δ as compared to *exo1*Δ (Figure 4C), which contrasts with the large (>10-fold) increase in reads throughout the sequencing window further from the DSB in the double mutant (Figure 4B,D). We observed intermediates mapping to positions throughout our

sequencing window without a drop off in signal, which indicates that Mre11 is resecting past the point of detection for this assay (~350 bp), even when we extended our window to include reads mapped to the common sequence shared with the control allele (Supplementary Figure 4). The massive increase in signal in *exo1*Δ *sgs1*Δ clearly exposes a transition point at approximately position -119 (Figure 4B,D). DSB-proximal to this point, the presumptive actions of Mre11 are restricted to only a few selected positions that have a limited periodicity. After -119 bp, the resection pattern shifts in both *exo1*Δ *sgs1*Δ and *exo1*Δ to one indicative of a kinetically slower process, since once again cleavage at the more distal positions would prevent detection of simultaneous cleavage at the more proximal positions. It is noteworthy that major peaks occur position -208 and -294 in the double mutant, which may represent further stepwise incisions generated by Mre11.

**Mre11 endonucleolytic activity is influenced by DNA sequence preferences**

Broadly, three mechanisms might dictate the specific resection profiles seen above: (i) proteins might "measure" cleavage positions relative to the DSB end, (ii) pre-damage factors such as nucleosomes or other bound proteins might constrain repair protein action, or (iii) repair proteins themselves might show a driving sequence dependence. To distinguish these in our system, we made two deletions near the -65/-66 position in WT and *exo1*Δ backgrounds (Figure 5A,C). The deletions each removed three base pairs either 31-33 or 71-73 bp away from the HOcs, i.e. DSB proximal and distal to the -65/-66 position, respectively. Strikingly, the DSB-proximal deletion led to a -3 bp shift in the position of the Mre11-dependent peak in both WT and *exo1*Δ cells, meaning that the same underlying sequence was being cleaved by the Mre11 nuclease even thought it was now closer to the DSB end (Figure 5B). Somewhat unexpectedly, the deletion distal to the -65/-66 position changed the pattern of peaks at from -60 to -66, possibly due to

their close proximity (Figure 5D). Both deletions further shifted the resection pattern throughout the distal portions of the sequencing window, including the Exo1-dependent -206 bp position in WT cells and the -119 position in *exo1*Δ (Supplementary Figure 5). Thus, the signal patterns throughout the interrogation window proved to be highly sequence, not distance, dependent.

**Sequencing of 5' endpoints formed from both DSB ends**

To expand our base of observation for the above findings we next examined the opposite side of the *ILV1* DSB using the same conceptual approach as in Figure 1. Because this 2$^{nd}$ side of the DSB corresponds to the *ILV1* coding region, we refer to it as *ILV1*-CR and the sequence studied above as *ILV1*-PR, for "promoter" (Figure 6A). We observed a higher background in WT and *exo1*Δ cells for *ILV1*-CR, but a similar overall pattern was observed on either side of the break (Figure 6B). Intriguingly, a number of reads lined up at the *ILV1*-CR -206 bp position in both WT and *exo1*Δ cells. Of primary note was that a peak appeared at -70 bp for *ILV1*-CR and not at -65/-66 bp as for *ILV1*-PR, consistent with the sequence, not distance, dependence noted above. Indeed, analysis of the underlying sequence, oriented similarly with respect to the DSB, revealed a similar palindromic "TCT" motif, with the cytosine being an efficient incision point (Figures 6C,D).

To examine the nucleotides contributing to the *exo1*-dependent rise in resection signal in both sequencing windows, we first set a cut-off value of 10% of the highest number of unique reads counted at one position in each *exo1*Δ mutant. We then took the DNA sequence surrounding these 5' terminated endpoints and generated logo plots (Figure 6E). We did observe a slight consistent preference for A or G in the position immediately before the 5'-terminated endpoint in Exo1-deficient cells. Even though this sequence-specific signal was weak, it is

noteworthy because it is different that the putative motif noted above and thus implicates a non-Mre11-dependent mechanism for these various signal peaks.

**NHEJ and other repair factors influence resection initiation near the DSB terminus**

To gain further insight into the obstacles that Mre11 faces near the DSB terminus, we deleted the NHEJ genes *YKU70* and *NEJ1* and analyzed early resection sequencing intermediates. The signal at position -65/-66 persisted in *yku70*Δ, indicating that Ku binding to a DSB end is not uniquely responsible for this Mre11-dependent cleavage position (Figure 7A). We did notice that the more proximal -42 bp peak became more prominent in *yku70*Δ, however. Moreover, loss of Ku created an interesting change near the DSB wherein WT showed a progressive increase in signal over time whereas *yku70*Δ had a nearly constant signal (Figure 7B), which might suggest an easier movement of resection inward from the DSB end. More drastic was the decrease in reads aligning near the HOcs in *nej1*Δ, which may also signify an increase in the kinetics of resection initiation.

Finally, examination of factors involved in supporting cleavage by Mre11 revealed a large increase in reads aligning near the HOcs in *sae2*Δ and *tel1*Δ (note the scale difference between WT and these mutants in Figure 7B) and the same near absence of reads at -65/-66 bp as in *mre11Δ* mutants. These results confirm a slower 5' degradation process from the DSB end in the absence of Mre11 nuclease activity, specifically at the Exo1-dependent -2 position.

## Discussion

End resection is a fast process occurring at a rate of 4 kb/h (31). However, HR must overcome multiple obstacles close to the DSB that dictate the successful transition to long-range resection (36). One obstacle is repair by NHEJ. We exploited catalytically defective Dnl4 to remove this competing outcome while maintaining normal Ku and DNA ligase IV assembly at DSB ends (29). Despite these obstacles, >20% of HO-cut *ILV1* alleles were resected past our ~350 bp sequencing window within 60 minutes of suffering the DSB. Resection steadily increased to 90 minutes but was associated with only limited detectable 5'-endpoint patterns in strains that were wild-type for resection-associated genes. Thus, while resection was clearly initiating in the sequenced regions during the experiment, the transition to progressive long-range resection was normally kinetically very fast once initiated.

Mutations further revealed important features of the observed patterns, where interpretations are guided by the following principles. When a signal peak is observed, we infer that there is a relative delay in processing at that base position. When a strain alteration causes such a signal to increase that delay has been accentuated, which implicates the altered protein as being responsible for the normal processing away from that 5'-terminated intermediate. In contrast, decreased signal in response to a strain alteration suggests that the protein factor normally creates the signal; such an intermediate can sometimes be inferred to be the product of a nuclease's action. However, a caveat is that primer extension only reveals the most DSB-distal 5' cleavage point on a DNA strand, so that DSB-proximal increases could result from decreased endonucleolytic activity more distally and vice versa.

Unlike our base *dnl4*-K466A mutation, *yku70* and *nej1* mutations removed the Ku and Nej1 NHEJ factors thought to be inhibitory to resection (17, 37). The greatest effect of these

losses was indeed to decrease the signal near the DSB. Thus, Ku and Nej1 might be seen as normally impeding further processing away from these positions. Loss of Nej1 had the largest impact and reduced signals to near-background levels, consistent with it limiting end-processing capable of initiating resection (38). An alternative interpretation is that the DSB-proximal signals are not resection intermediates but instead reflect processing associated with futile attempts at NHEJ. These are not exclusive concepts and the fact that signal at the prominent -2 position failed to accumulate in Ku mutant yeast suggests that NHEJ factors might normally but only temporarily stabilize DSB-proximal intermediates. Notably, signal at the -2 position was uniquely dependent on Exo1, which identifies Exo1 as the nuclease that cleaves to some, but not all, of the DSB-proximal 5' intermediates (39). In contrast to Ku and Nej1, loss of Mre11 or its nuclease activity led to increased signal at the DSB-proximal positions, most profoundly at -2 bp, with a similar result upon loss of the Tel1 and Sae2 proteins that support Mre11 (10, 16, 40). Here, the best interpretation is that the signal increase is secondary to decreased DSB-distal endonucleolytic cleavage.

Moving inward from the DSB end we find the most critical region for resection initiation. Previous *in vitro* analysis of Mre11 activity on Ku-occluded dsDNA substrates revealed incisions at 35-45 and 55-65 bp from the end on 70 and 100 bp substrates, respectively (22, 41), leading to the prevailing model wherein Mre11 creates a nick at a distance enforced by the Ku protein block (23). We observed a pattern of iterative peaks throughout this region consistent with the model and with the inference of a "stepwise" cleavage at somewhat regularly spaced positions (24). Although subtle, the pattern of three *ILV1*-PR peaks at -42, -65/-66 and –84 bp positions was evident in wild-type yeast and enhanced upon loss of Exo1. That increase was strongly dependent on the Mre11 nuclease as evidenced by absence of -65/-66 signal in an *exo1 mre11-*

H125N double mutant. The relative weaknesses of the -42 signal could be secondary to cleavage at -65/-66, but -84 had substantially lesser cleavage activity.

A central question is what determines the pattern of cleavage at mitotic DSBs *in vivo*. Models cited above imply that Ku and/or Mre11 protein sizes are critical factors (22, 23, 41), but the pattern could be enforced by other proteins bound prior to damage such as histones or other proteins (42, 43) and DNA repair proteins are can have sequence-specific properties (44, 45). We addressed these issues using 3 bp deletions in the *ILV1*-PR sequence. Strikingly, the -65/-66 peak moved closer to the DSB with the DSB-proximal deletion and thus tracked the local sequence, not the distance from the DSB end. Further evidence for sequence specificity comes from the identification of a similar incision position at -70 bp on the *ILV1*-CR side of the DSB whose sequence shared 5 out of 7 bases with the *ILV1*-PR -65/-66 peak. Critically, this predominant cleavage position did not move in *yku70* mutant yeast but the -42 position did become the most prominent. Thus, we conclude that Ku itself is not the primary factor leading to the position of the inferred Mre11 incisions but that it may impede access to the more DSB-proximal positions.

It is equally important to consider where resection intermediates were not observed, which was especially noticeable in *exo1 sgs1*, a strain deficient in long range resection thought to mainly support cleavage by Mre11 (35). Resection initiation signal with this strain increased dramatically, although the signal at -65/-66 was only modestly increased relative to *exo1*. Indeed, most positions up to -119 bp had limited read counts despite the poor ability to transition to progressive resection. We infer that the first ~100 bp of a DSB are a unique zone where a specific protein “footprint” protects the DNA from promiscuous activity. The source of that protection is not entirely clear but is not Ku, Sgs1, or Exo1. It might be MRX itself, although this is difficult to prove with resection data alone.

The genesis of signal after -119 bp is intriguing. In yeast with Exo1 and Sgs1 it is dependent on the Mre11 nuclease, consistent with the later peaks, especially the strong and specific -206 position, resulting from exonucleolytic extension away from the more proximal incisions. Consistently, the -206 signal was abrogated in *exo1* yeast identifying it as a pause point during extension by Exo1. We do not know the nature of the obstacle that causes Exo1to pause but a strong candidate is the 9-1-1 complex based on recent observations (35). Whatever is responsible is again sequence specific as the location of the peak shifted with the DSB-proximal 3 bp deletions. The large increase in signal past -119 bp in *exo1 sgs1* yeast is uncertain; it might be a result of more distal, kinetically slower and pathologic cleavage by Mre11 but we were unable to make an *exo1 sgs1 mre11*-H125N triple mutant to test this idea (19).

A caveat is the possibility for artifacts arising from the use of the HO endonuclease. HO can remain bound to its cleavage product (46) so we cannot rule out that HO itself is partially responsible for the observed cleavage patterns, although all DSB repair actions occur at HO DSBs and we make our measurements long after repair proteins have engaged the DSB. We also considered whether HO might cleave off-target to create some measured endpoints, especially when the DSB was resistant to resection (47). Importantly, we never saw anything above a low baseline cleavage at the control allele. Also, many cleavage intermediates could be abrogated by repair mutations identifying them as specific. However, one peak at –294 in *exo1 sgs1* yeast had possible sequence similarity to the HOcs and could represent “skipping” of HO to this alternative position (Supplementary Figure 6).

Our results align with those who have used sequencing approaches to study meiotic end resection. Notably, we observed increased intermediates throughout our sequencing window in *exo1* cells that mirrors the effect reported by the Keeney group (27). Our data also support that

Tel1 promotes efficient resection and a decrease in unique reads mapping near the DSB termini. Keeney described evidence of Exo1-dependent pausing at heterochromatin but it is uncertain how closely that phenomenon corresponds to our precise Exo1 pause point.

In summary, results here provide a uniquely high-resolution picture of mitotic DSB resection initiation. They support published models in which Ku and Nej1 inhibit exonucleolytic resection from the DSB end in a manner that is overcome by Mre11 incision with a peak activity ~60 to 70 bp from the DSB end. This is followed by rapid nick extension by predominantly Exo1 that is processive but also subject to pausing. However, the cleavage pattern is complex, substantially sequence dependent, and influenced by an inferred protective protein complex that is not strongly dependent on Ku. Critical challenges are to extend these findings across many DSBs and to correlate DNA-based results with equally high-resolution protein binding studies *in vivo* to understand the nature of the early mitotic repair protein complex.

## Materials and Methods

### Yeast strains and growth media

Haploid yeast were grown at 30 C in either rich medium containing 1% yeast extract, 2% peptone and 40 μg/ml adenine (YPA) with either 2% glucose, 2% galactose, or 2% glycerol as a carbon source. Yeast strains were isogenic derivatives of BY4741 (48). The base strain for most strains used in this study was YW3104, itself a derivative of YW1405 that has been previously described (28). All additional gene disruptions and modified alleles were made using a polymerase chain reaction (PCR)-mediated technique or a *URA3* pop-in/pop-out method and confirmed by PCR and sequencing (49). A table of all yeast strains is provided as Supplementary Table 1.

Relative to YW1405, YW3104 bears three additional genetic alterations. A *bar1* mutation promoted efficient G1 synchronization by α-factor. A previously described point mutation, *dnl4*-K466A abrogated activity of the yeast NHEJ ligase (29). The third change at the *ILV1* locus and was made to introduce the NdeI site and other sequences used in most experiments; its exact content was related to a prior design concept that was abandoned and not discussed here. Specifically, we inserted a bacterial *ori* sequence followed downstream by the *HIS3-MX6* selection marker at a genomic location 802 bp upstream of the *ILV1* HOcs. The fourth change in all strains that were subjected to sequencing-based resection monitoring was the addition of a control allele, which was always the last construction step to yield paired strains with and without the control allele. For this purpose, we identified an appropriate native RE site in the genome (e.g. NdeI) and inserted a construct containing homology to *ILV1* 350 bp upstream of the RE cleavage site with *URA3* as a selection marker. This construct was homologous to the portion of *ILV1* that is needed for primer extension and library amplification but lacks the HOcs.

**Oligonucleotide primers and probes**

Oligonucleotide primers and probes were from IDT. A complete list of all sequences is provided in Supplementary Table 2. All primers bore 5' hydroxyls. Primer extension primers were made with hand-mixed UMIs at an equal percentage of A,C,G,T and a series of 6 different known and fixed time point barcodes. They were designed to anneal to the RE site DBS-distal to the HOcs such that primer extension reaction would copy both the 5' primer tail (from the genomic DNA 3' end) and the genomic DNA (from the primer 3' end). Replicate time courses from the same strain always used different primer extension primers to ensure that the time point barcodes did not create an unanticipated bias.

**DSB induction paradigm**

Strains containing the *ILV1* HOcs with and without the control allele were grown separately overnight at 30 C to saturation in YPA-dextrose media then inoculated to a low $OD_{600}$ in YPA-glycerol for a consecutive night. When the $OD_{600}$ of the YPA-glycerol cultures was in the range of 0.3 to 0.6, the strain with the control allele was spiked into the other YPA-glycerol culture at a ratio of 1:20 as determined by $OD_{600}$. The T0 time point was taken by rapidly mixing 45 mL of this YPA-glycerol culture into 5 mL 0.5 M EDTA to quickly quench cellular nuclease activities. Galactose was then added to the YPA-glycerol culture at 2% final concentration to induce HO expression and DSB formation. Another time point was taken 35 minutes after galactose addition in the same fashion as T0. At 45 minutes after galactose addition the YPA-glycerol+galactose culture was pelleted and the cell resuspended in an equal volume of YPA-dextrose followed by continued shaking at 30 C. Further time points were taken as above at 60, 75 and 90 minutes after galactose addition (15, 30 and 45 minutes after the switch to dextrose, respectively). Time course materials used in ddPCR-based resection monitoring were generated by a similar protocol

but without the control allele spike-in and only 1.5 mL of cellular extract was taken from a smaller total growing culture volume without EDTA addition.

**Genomic DNA preparation and quality validation**

High molecular weight gDNA was obtained using the Thermo Scientific Pierce Yeast DNA Extraction Kit. Yeast cells were thus lysed without glass beads or damaging chemical treatment. Genomic DNA was subjected to 0.8% agarose gel electrophoresis to confirm its high molecular weight and purity (Supplementary Figure 2).

**Resection monitoring by RE-ddPCR**

To measure resection flux through the interrogation window of our sequencing method, we used a ddPCR method based on resistance of ssDNA to RE cleavage. That method is described in detail in Lomonaco et al (https://biorxiv.org/cgi/content/short/2021.02.26.433101v1). Briefly, HinfI was used to digest the gDNA from the smaller 1.5 mL cultures. HinfI cleavage was confirmed by gel electrophoresis. ddPCR measurements using probes targeting a HinfI site 355 bp from the HOcs and an *ACT1* control locus revealed when the HinfI site became resistant to cleavage due to resection.

**Resection monitoring by high resolution primer extension sequencing**

<u>Quantification of DNA amount and the exact control allele ratio</u>

gDNA was quantified and HOcs curves were established using a dual fluorophore ddPCR assay with primers flanking the HOcs (FAM) and within the undamaged reference gene, *ACT1* (VIC). The fraction of uncut alleles was directly measured as the fraction of molecules giving signal with the HOcs relative to the *ACT1* probes. The true control allele spike-in percentage was further established in the sequencing assay using DNA extracted from the T0 sample, i.e. prior to DSB formation. Importantly, all further time points were taken from the exact same culture so

the value from the T0 specimen applied equally well to later time points also. That assay used paired probes homologous to the control allele (only present in the spiked-in cells) and the HOcs-containing *ILV1* locus (present in all cells regardless of whether they had the control allele, i.e. all cells in the culture made the same DSB).

Restriction enzyme digestion, primer extension and intramolecular ligation

Twenty micrograms of gDNA was digested by 40 units of NdeI (NEB) in Cutsmart Buffer at 37 C for one hour. The tubes were then incubated at 65 C for 20 minutes to deactivate NdeI. The digested DNA was purified using AMPure XP Beads and eluted using water. The primer extension reaction used 1 unit of Phusion DNA polymerase and a custom primer containing a fixed 6 nt time point barcode sequence, 12 nt hand-mixed UMIs and several single fixed nucleotides used to locate the UMIs (see below). Primer extension and tagging of molecules was done separately in each time point with different fixed 6 bp barcode sequences. The uncycled extension reaction had the following conditions: 98 degrees for 3 minutes, 55 degrees for 3 minutes, 72 degrees for 10 minutes. The extended molecules from each time point were purified using AMPure XP and eluted using water. Intramolecular ligation was then carried out overnight at room temperature in a diluted T4 DNA Ligase reaction at a concentration of 20 U/µL. The ligase was then inactivated at 65 C for 10 minutes.

Amplification and sequencing of custom library

Once UMIs had been covalently ligated to gDNA 5' endpoints and the ligase inactivated, all time point samples from a given culture's time course were pooled together and purified using AMPure XP beads. Therefore, any bias due to PCR amplification and sequencing was expected to apply equally to all time points. Specifically, ligation junctions were amplified with primers flanking the HOcs that were tailed with sequences homologous to Illumina P5 (DSB side) and P7

(upstream NdeI side) adapters used in high-throughput sequencing. This PCR used KAPA HiFi HotStart Polymerase with the following conditions: 95 C for 3 minutes, 17 cycles of 98 C for 20 seconds, 60 C for 15 seconds, 72 C for 30 seconds, and finally 72 C for 1 minute. Products were purified on AMPure XP beads then a custom Illumina amplicon library was made through PCR using IDT Illumina-compatible i5 and i7 indexed adapters, which identified the time course, i.e. source sample culture. The second adapter PCR also used KAPA HiFi with the following conditions: 95 C for 3 minutes and 8 cycles of 95 C for 30 seconds, 55 C for 30 seconds, 72 C for 30 seconds. Ten individual custom amplicon libraries, each representing one complete time course series, were submitted to the University of Michigan Advanced Genomics Core where they were balanced, pooled and sequenced on 2.5% of a shared Illumina Novaseq lane in the 2 x 151 format.

**Bioinformatics analysis**

Code and support file availability

All code and support files required to execute data analysis are available from GitHub at https://github.com/wilsonte-umich/resection-seq. The pipeline was executed using the q pipeline manager available at https://github.com/wilsonte-umich/q-pipeline-manager. Briefly, a q data file is written to establish values for sample- and server-specific variables, which then invokes repository file ‘resection-seq/process_sample.q’ via command ‘q submit <data-file>.q’.

Each DSB end to be profiled required an indexed FASTA file with the sequence of the reference and control alleles, plus Perl and R scripts defining their structures. Files for all DSBs used in this study are provided in repository directory ‘resection-seq/Bazzano_2021/references’. Each sample to be analyzed required a row entry in a metadata file that described the

experiments and time points; a complete file for all samples in this study is provided as 'resection-seq/Bazzano_2021/ResectionMasterStrainTable.txt'.

Read validation and alignment

Data from the sequencing core consisted of paired end reads that had been de-multiplexed per sample using the Illumina indices added in the last PCR step but that still had a mixture of all time points per sample. Read 2 (from the P7 primer) was only needed for sample demultiplexing and was not used further. Each read 1 from the P5 primer was analyzed to determine if it matched in read order (i) an appropriately long leader sequence corresponding to the DSB-distal end of the resected fragment, (ii) a UMI of the appropriate length, (iii) a single fixed A base, (iv) a known 6 bp time point barcode, (v) two fixed TA bases, and finally (vi) sequence corresponding to the DSB-proximal or control-proximal DNA that had been ligated to the UMI during circularization. Reads that failed to match this pattern were discarded.

For matching reads, 36 bp of the proximal sequence was extracted and aligned to the DSB and control reference sequences using Bowtie (50) with options '-v 3 -k 1 -m 1 –best', such that only unique alignments with up to three mismatches were accepted (some reads were expected to map twice to the common sequence shared between the DSB and control alleles). Productive alignments were sorted and grouped by all unique combinations of time point, UMI sequence, and alignment position, which acted as the definitive molecule identifier (a UMI could be used by more than one time point because those libraries were prepared separately and by more than one mapped position because different positions were distinctive based on the strict alignment criteria). Metrics consistently confirmed high data quality, including that (i) there were <2% unaligned reads, (ii) reads only aligned to the predicted strand of the reference sequences, and (iii) >95% of reads aligned with no mismatches.

Purging redundant UMIs

We next accounted for PCR or sequencing errors introduced into UMIs that would lead to over-counting of the number of truly unique source molecules. We used custom code to implement the directional model of Smith et al. (51), which considers a UMI network to have originated from the UMI node with the highest counts, with UMIs added to an existing network if they have at most 1 mismatch from a UMI already in the network. Repository script 'collapse/collapse_UMIs.R' implements an efficient algorithm for solving such networks that matched our data needs, given that we expected very large numbers of unique molecules mapping to a few specific alignment positions. The algorithm exploits 2-bit encoding of all possible UMI sequences and pre-calculated XOR values for all UMI pairs with a Hamming distance of 1. See script for details.

Our 12 bp UMIs did not always have sufficient diversity to avoid UMI collisions for the HO or RE-cut ends of the DSB allele; accordingly, for this reason and for computational speed we disregarded DSB allele positions that had more than 500K mapped molecules, which always included the DSB end itself. In contrast, all positions were always subjected to UMI analysis for the control allele, which had been doped into the yeast pool at a nominal fraction of 5% so that UMI collisions were expected to be minimal. The result was a reduction in molecule counts per unique combination of time point, UMI sequence, and alignment position to reflect only true inferred source molecules.

Discarding failed libraries

To identify poorly performant libraries we wrote repository script ''resection-seq/parse_q_report.pl' to read the output of 'q report -j all <data.file>.q' and write a table with summary statistics of all samples. The output is provided for all samples in this study as

repository file ‘resection-seq/Bazzano_2021/ResectionOutputSummary.xlsx’. It allowed us to establish criteria that a time point library needed to have at least 3.5M cell equivalents of input DNA, as determined by the corrected control molecule count, and a background breakage frequency less than 0.03% in the control allele. Libraries failing these criteria were written to repository file ‘resection-seq/Bazzano_2021/BadLibraryTable.txt’ to allow the R server code below to mask them. Because time point libraries were initially handled separately, a sample could have many successful time points even if one failed.

Assembly, normalization and visualization

For each sample we cross-tabulated read counts such that mapped positions were in rows and time points in columns and wrote two R Shiny web tools to analyze these tables, provided in repository directory ‘resection-seq/_server’; ‘visualize’ creates scatterplots for a series of samples as a function of allele position whereas ‘heatmap’ creates plots of position by time point with values expressed by color intensity.

For each tool, the first normalization step was to sum the count of all unique control allele molecules, whether intact or fragmented, to establish the total number of control alleles (and thus haploid cell equivalents) present in the sequenced DNA. We next calculated the inferred number of DSB alleles present in the sequenced DNA by correcting that control allele count by the fraction of control allele-bearing cells in the sequenced mixture, determined by ddPCR from the time 0 specimen as described above. The fraction of all input alleles that mapped to each possible DSB or control allele position was calculated by dividing the molecule count at that position by the actual or inferred allele counts established above. Note that although degradation of the DSB allele could lead to lower total recovered counts at later time points, the

calculated fractions remained accurate because they were normalized to the control allele, which was unaffected by degradation.

The signal for the control allele was mostly at the NdeI restriction site (Supplementary Figure 3) but the signal at other control positions provided a means of assessing the extent and nature of random fragmentation that occurred in each DNA prep. This pattern included evidence that smaller PCR fragments were sometimes more highly represented in final libraries, so we characterized the background fragmentation by fitting a linear regression to the non-NdeI positions of the control allele. The fraction predicted by that regression was then subtracted from the fraction values at all DSB positions to establish our final normalized values for DSB allele positions, referred to as "signal above control" or "DSB – control". Examination of samples at time 0 consistently validated this approach, i.e. that the control allele regression line was an excellent model for background fragmentation of the DSB allele (Supplementary Figure 3). Accordingly, the normalized fractional DSB signal above control consistently averaged to zero prior to DSB formation and only rose after the DSB was formed.

Finally, normalized values were averaged for each time point over all samples of the same culture type (e.g. WT). Heatmaps applied a linear color transformation to the averaged DSB signal above control; the scale of all plots is provided in the figures. The value can be negative due to random fluctuations but is never expected to have large negative values.

Logo plots

Logo plots were generated using the web service http://weblogo.threeplusone.com/.

**Data availability**

FASTQ files with sequencing reads are available for all samples from the NIH Sequence Read Archive via accession PRJNA703820 (temporary Submission ID: SUB9120849).

**Acknowledgements**

This work was supported by NIH grant R01 GM120767 to T.E.W and a supplement of the same number awarded to S.L. The authors thank Olivia Koues and the staff of the Michigan Advanced Genomics Core for advice and expert handling of high throughput sequencing services. We also thank Christian Rizza for his work assembling the RE-ddPCR-based resection plots.

**Conflicts**

The authors declare that they have no competing financial interest with this work.

## Figure Legends

**Figure 1. Description and validation of resection sequencing by primer extension and circularization.**

**(A)** *ILV1* DSB formation efficiency as determined by ddPCR after galactose addition at time 0 to induce HO expression. **(B)** ddPCR-based resection assay to determine the percentage of ssDNA after DSB induction at a site 355 bp away from the HOcs. When indicated, cells were washed into glucose at 45 minutes (arrow). **(C)** Steps in resection sequencing to map 5' terminated end intermediates at base-pair resolution using primer extension to add UMIs, followed by intramolecular circularization and PCR of junctions. **(D)** Library products were sequenced such that an indexed P5 primer read, in order, the UMI, a fixed time point barcode and genomic bases from the *ILV1* DSB or a control locus. **(E)** Heatmap depicting the fraction of unique molecules with 5' endpoints at each position on one side of the *ILV1* HOcs, expressed as a normalized signal above the background fraction of reads aligning to the control locus at similar fragment sizes (see Methods). The NHEJ-defective Dnl4 catalytic point mutant *dnl4*-K466A is considered WT with respect to resection. **(F)** Bar graph showing the fraction of unique *ILV1* molecules with 5' ends within the first 10 bp away from the HOcs for each time point in WT. Negative position designations indicate the number of bases removed from the 5' terminated strand. Bars are the average +/- standard deviation of four biological replicates. **(G)** Expansion of the region from (E) -30 to -90 bp from the HOcs in WT. The color scale is 2-fold more sensitive than (E).

**Figure 2. Loss of Exo1 increases resection signal close to the *ILV1* DSB, especially at -65/-66 bp.**

**(A)** Heatmaps of resection signal similar to Figure 1E for WT, *exo1*Δ and *sgs1*Δ yeast. **(B-D)** The normalized fractional resection signal above background is plotted for WT, *sgs1*Δ and *exo1*Δ yeast at positions **(B)** -1 to -10 bp, **(C)** -60 to -70 bp and **(D)** -204 to -215 bp from the *ILV1* HOcs on the promoter side of the gene. Exo1 loss had opposite effects on the signal obtained at the -2 and -206 positions as compared to the -65/-66 bp peak.

**Figure 3. Mre11 nuclease activity is necessary to form resection intermediates at -65/-66 bp.**

**(A)** The first three panels show heatmaps of resection signal for WT, *mre11*Δ and catalytically defective *mre11*-H125N strains in the first 125 bp from the HOcs. The next two panels plot the difference between the WT and mutant strains to highlight where signal was higher (red) or lower (blue) in WT as compared to mutant. **(B)** Fractional resection signal at positions -203 to -209 bp in WT, *mre11*Δ and *mre11*-H125N strains at the 90 minute time point. **(C)** Heatmaps of resection signal for *exo1*Δ and *mre11*-H125N *exo1*Δ yeast up to 300 bp from the HOcs. **(D)** ddPCR-based resection analysis of WT and mutant strains at a site 355 bp from the HOcs. Points are the average of two biological replicates. **(E&F)** Fractional resection signal 60 minutes after DSB induction in WT, *exo1*Δ and *mre11*-H125N *exo1*Δ yeast at positions **(E)** -1 to -20 bp and **(F)** -60 to -70 bp from the HOcs.

**Figure 4. Exo1- and Sgs1-deficient yeast show greatly enhanced resection intermediates beyond position -119.**

**(A**) ddPCR-based resection analysis of WT and mutant strains at a site 355 bp from the HOcs with combinations of *exo1* and *sgs1* deletions. **(B)** Heatmaps of resection signal for *exo1*Δ and *exo1*Δ *sgs1*Δ yeast. The uniquely mappable *ILV1* sequences end at position -344. **(C)** Fractional resection signal surrounding the -65/-66 bp position for *exo1*Δ and *exo1*Δ *sgs1*Δ yeast. The same y-axis scaling is used on both graphs. **(D)** Fractional resection signal for the first 300 bp away from the DSB for each time point in *exo1*Δ and *exo1*Δ *sgs1*Δ yeast. Note the large increase in y-axis scaling in the *exo1*Δ *sgs1*Δ plot due to the accumulation of many more intermediates in this strain background.

**Figure 5. The predominant Mre11-dependent incision shows sequence dependence more than a strict positional dependence.**

**(A)** Diagram of a 3 bp deletion in *ILV1* located 31-33 bp from the HOcs. **(B)** Fractional resection signal from positions -20 to -100 in WT and *exo1*Δ yeast 90 minutes after DSB induction with and without the 3 bp deletion at positions -31 to -33. Vertical dashed lines in the top plot mark the location of the positions that were deleted in the bottom plot. A vertical blue line indicates the position expected for the peak in the bottom plot if the distance from the DSB end had been maintained after the 3 bp deletion. **(C)** Diagram of a 3 bp deletion in *ILV1* located 71-73 bp from the HOcs. **(D)** Similar to (B) for the 3 bp deletion located at positions -71 to -73.

**Figure 6: Comparing two sides of the *ILV1* DSB reinforces sequence dependence more than a strict positional dependence.**

**(A)** Sequencing scheme to capture intermediates resecting into the *ILV1* coding region (*ILV1*-CR; Figures 1-5 examined resection into the *ILV1* promoter region, *ILV1*-PR). **(B)** Heatmaps of resection signal up to 300 bp from the HOcs in WT and *exo1*Δ strains sequenced from either *ILV1*-PR or *ILV1*-CR in separate libraries. The scale for *ILV1*-CR strains is 2-fold less sensitive due to higher background levels. **(C)** Fractional resection signal at positions -60 to -70 bp in WT and *exo1*Δ yeast sequenced from *ILV1*-PR. The sequence of the 5' terminated strand is shown on the upper X-axis. **(D)** Fractional resection signal at positions -65 to -75 in WT and *exo1*Δ yeast sequenced from the *ILV1*-CR, with the sequence as in (D). **(E)** Logo plot analyzing sequences +/- 5 bp in either direction from signal peaks in *exo1*Δ yeast sequenced from either *ILV1*-PR or *ILV1*-CR. A threshold of 10% of the max peak height was used to determine the plotted peaks: *ILV1*-PR n=75, *ILV1*-CR n=67.

**Figure 7: NHEJ factors limit processing events near the DSB end**

**(A**) Heatmaps of resection signal within 100 bp of the *ILV1*-PR HOcs in WT and various single deletion mutants. **(B)** Fractional resection signal within the first 15 bp after the *ILV1*-PR HOcs for the same mutants as in (A).

## References


1. Scully R, Panday A, Elango R, & Willis NA (2019) DNA double-strand break repair-pathway choice in somatic mammalian cells. *Nature reviews. Molecular cell biology* 20(11):698-714.
2. Aparicio T, Baer R, & Gautier J (2014) DNA double-strand break repair pathway choice and cancer. *DNA repair* 19:169-175.
3. Strathern JN, *et al.* (1982) Homothallic switching of yeast mating type cassettes is initiated by a double-stranded cut in the MAT locus. *Cell* 31(1):183-192.
4. Chi X, Li Y, & Qiu X (2020) V(D)J recombination, somatic hypermutation and class switch recombination of immunoglobulins: mechanism and regulation. *Immunology* 160(3):233-247.
5. Chapman JR, Taylor MR, & Boulton SJ (2012) Playing the end game: DNA double-strand break repair pathway choice. *Molecular cell* 47(4):497-510.
6. Zhao B, Rothenberg E, Ramsden DA, & Lieber MR (2020) The molecular basis and disease relevance of non-homologous DNA end joining. *Nature reviews. Molecular cell biology* 21(12):765-781.
7. Emerson CH & Bertuch AA (2016) Consider the workhorse: Nonhomologous end-joining in budding yeast. *Biochemistry and cell biology = Biochimie et biologie cellulaire* 94(5):396-406.
8. Frit P, Ropars V, Modesti M, Charbonnier JB, & Calsou P (2019) Plugged into the Ku-DNA hub: The NHEJ network. *Progress in biophysics and molecular biology* 147:62-76.
9. Myler LR, *et al.* (2017) Single-Molecule Imaging Reveals How Mre11-Rad50-Nbs1 Initiates DNA Break Repair. *Molecular cell* 67(5):891-898.e894.
10. Cassani C, *et al.* (2019) The ATP-bound conformation of the Mre11-Rad50 complex is essential for Tel1/ATM activation. *Nucleic acids research* 47(7):3550-3567.
11. Williams RS, Williams JS, & Tainer JA (2007) Mre11-Rad50-Nbs1 is a keystone complex connecting DNA repair machinery, double-strand break signaling, and the chromatin template. *Biochemistry and cell biology = Biochimie et biologie cellulaire* 85(4):509-520.
12. Käshammer L, *et al.* (2019) Mechanism of DNA End Sensing and Processing by the Mre11-Rad50 Complex. *Molecular cell* 76(3):382-394.e386.
13. Zhang Y, *et al.* (2007) Role of Dnl4-Lif1 in nonhomologous end-joining repair complex assembly and suppression of homologous recombination. *Nature structural & molecular biology* 14(7):639-646.
14. Wilson TE, Grawunder U, & Lieber MR (1997) Yeast DNA ligase IV mediates non-homologous DNA end joining. *Nature* 388(6641):495-498.
15. Symington LS (2016) Mechanism and regulation of DNA end resection in eukaryotes. *Critical reviews in biochemistry and molecular biology* 51(3):195-212.
16. Cannavo E & Cejka P (2014) Sae2 promotes dsDNA endonuclease activity within Mre11-Rad50-Xrs2 to resect DNA breaks. *Nature* 514(7520):122-125.
17. Chanut P, Britton S, Coates J, Jackson SP, & Calsou P (2016) Coordinated nuclease activities counteract Ku at single-ended DNA double-strand breaks. *Nature communications* 7:12889.

18. Cejka P (2015) DNA End Resection: Nucleases Team Up with the Right Partners to Initiate Homologous Recombination. *The Journal of biological chemistry* 290(38):22931-22938.
19. Mimitou EP & Symington LS (2008) Sae2, Exo1 and Sgs1 collaborate in DNA double-strand break processing. *Nature* 455(7214):770-774.
20. Garcia V, Phelps SE, Gray S, & Neale MJ (2011) Bidirectional resection of DNA double-strand breaks by Mre11 and Exo1. *Nature* 479(7372):241-244.
21. Bonilla B, Hengel SR, Grundy MK, & Bernstein KA (2020) RAD51 Gene Family Structure and Function. *Annual review of genetics* 54:25-46.
22. Reginato G, Cannavo E, & Cejka P (2017) Physiological protein blocks direct the Mre11-Rad50-Xrs2 and Sae2 nuclease complex to initiate DNA end resection. *Genes & development* 31(23-24):2325-2330.
23. Wang W, *et al.* (2018) A DNA nick at Ku-blocked double-strand break ends serves as an entry site for exonuclease 1 (Exo1) or Sgs1-Dna2 in long-range DNA end resection. *The Journal of biological chemistry* 293(44):17061-17069.
24. Cannavo E, Reginato G, & Cejka P (2019) Stepwise 5' DNA end-specific resection of DNA breaks by the Mre11-Rad50-Xrs2 and Sae2 nuclease ensemble. *Proceedings of the National Academy of Sciences of the United States of America* 116(12):5505-5513.
25. Peng H, Zhang S, & Chen X (2021) Monitoring 5'-End Resection at Site-Specific Double-Strand Breaks by Southern Blot Analysis. *Methods in molecular biology (Clifton, N.J.)* 2196:245-255.
26. Zhou Y, Caron P, Legube G, & Paull TT (2014) Quantitation of DNA double-strand break resection intermediates in human cells. *Nucleic acids research* 42(3):e19.
27. Mimitou EP, Yamada S, & Keeney S (2017) A global view of meiotic double-strand break end resection. *Science (New York, N.Y.)* 355(6320):40-45.
28. Wu D, Topper LM, & Wilson TE (2008) Recruitment and dissociation of nonhomologous end joining proteins at a DNA double-strand break in Saccharomyces cerevisiae. *Genetics* 178(3):1237-1249.
29. Chiruvella KK, Liang Z, Birkeland SR, Basrur V, & Wilson TE (2013) Saccharomyces cerevisiae DNA ligase IV supports imprecise end joining independently of its catalytic activity. *PLoS genetics* 9(6):e1003599.
30. Bawa G & Ghovanloo M (2008) Active High Power Conversion Efficiency Rectifier With Built-In Dual-Mode Back Telemetry in Standard CMOS Technology. *IEEE transactions on biomedical circuits and systems* 2(3):184-192.
31. Zhu Z, Chung WH, Shim EY, Lee SE, & Ira G (2008) Sgs1 helicase and two nucleases Dna2 and Exo1 resect DNA double-strand break ends. *Cell* 134(6):981-994.
32. Gobbini E, *et al.* (2018) The MRX complex regulates Exo1 resection activity by altering DNA end structure. *The EMBO journal* 37(16).
33. Moreau S, Ferguson JR, & Symington LS (1999) The nuclease activity of Mre11 is required for meiosis but not for mating type switching, end joining, or telomere maintenance. *Molecular and cellular biology* 19(1):556-566.
34. Cejka P, *et al.* (2010) DNA end resection by Dna2-Sgs1-RPA and its stimulation by Top3-Rmi1 and Mre11-Rad50-Xrs2. *Nature* 467(7311):112-116.
35. Gobbini E, Casari E, Colombo CV, Bonetti D, & Longhese MP (2020) The 9-1-1 Complex Controls Mre11 Nuclease and Checkpoint Activation during Short-Range Resection of DNA Double-Strand Breaks. *Cell reports* 33(3):108287.

36. Marini F, Rawal CC, Liberi G, & Pellicioli A (2019) Regulation of DNA Double Strand Breaks Processing: Focus on Barriers. *Frontiers in molecular biosciences* 6:55.
37. Sorenson KS, Mahaney BL, Lees-Miller SP, & Cobb JA (2017) The non-homologous end-joining factor Nej1 inhibits resection mediated by Dna2-Sgs1 nuclease-helicase at DNA double strand breaks. *The Journal of biological chemistry* 292(35):14576-14586.
38. Mojumdar A, *et al.* (2019) Nej1 Interacts with Mre11 to Regulate Tethering and Dna2 Binding at DNA Double-Strand Breaks. *Cell reports* 28(6):1564-1573.e1563.
39. Gobbini E, Vertemara J, & Longhese MP (2018) Local unwinding of double-strand DNA ends by the MRX complex promotes Exo1 processing activity. *Molecular & cellular oncology* 5(5):e1511208.
40. Yu TY, Garcia VE, & Symington LS (2019) CDK and Mec1/Tel1-catalyzed phosphorylation of Sae2 regulate different responses to DNA damage. *Nucleic acids research* 47(21):11238-11249.
41. Wang W, Daley JM, Kwon Y, Krasner DS, & Sung P (2017) Plasticity of the Mre11-Rad50-Xrs2-Sae2 nuclease ensemble in the processing of DNA-bound obstacles. *Genes & development* 31(23-24):2331-2336.
42. Yu TY, Kimble MT, & Symington LS (2018) Sae2 antagonizes Rad9 accumulation at DNA double-strand breaks to attenuate checkpoint signaling and facilitate end resection. *Proceedings of the National Academy of Sciences of the United States of America* 115(51):E11961-e11969.
43. Li K, Bronk G, Kondev J, & Haber JE (2020) Yeast ATM and ATR kinases use different mechanisms to spread histone H2A phosphorylation around a DNA double-strand break. *Proceedings of the National Academy of Sciences of the United States of America* 117(35):21354-21363.
44. Rahal EA, *et al.* (2010) ATM regulates Mre11-dependent DNA end-degradation and microhomology-mediated end joining. *Cell cycle (Georgetown, Tex.)* 9(14):2866-2877.
45. Tadi SK, *et al.* (2016) Microhomology-mediated end joining is the principal mediator of double-strand break repair during mitochondrial DNA lesions. *Molecular biology of the cell* 27(2):223-235.
46. Jin Y, Binkowski G, Simon LD, & Norris D (1997) Ho endonuclease cleaves MAT DNA in vitro by an inefficient stoichiometric reaction mechanism. *The Journal of biological chemistry* 272(11):7352-7359.
47. Nickoloff JA, Singer JD, & Heffron F (1990) In vivo analysis of the Saccharomyces cerevisiae HO nuclease recognition site by site-directed mutagenesis. *Molecular and cellular biology* 10(3):1174-1179.
48. Brachmann CB, *et al.* (1998) Designer deletion strains derived from Saccharomyces cerevisiae S288C: a useful set of strains and plasmids for PCR-mediated gene disruption and other applications. *Yeast (Chichester, England)* 14(2):115-132.
49. Palmbos PL, Daley JM, & Wilson TE (2005) Mutations of the Yku80 C terminus and Xrs2 FHA domain specifically block yeast nonhomologous end joining. *Molecular and cellular biology* 25(24):10782-10790.
50. Langmead B, Trapnell C, Pop M, & Salzberg SL (2009) Ultrafast and memory-efficient alignment of short DNA sequences to the human genome. *Genome biology* 10(3):R25.
51. Smith T, Heger A, & Sudbery I (2017) UMI-tools: modeling sequencing errors in Unique Molecular Identifiers to improve quantification accuracy. *Genome research* 27(3):491-499.

# Figure 1

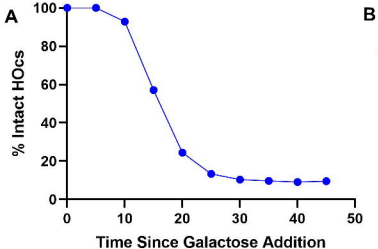
A
% Intact HOcs
Time Since Galactose Addition

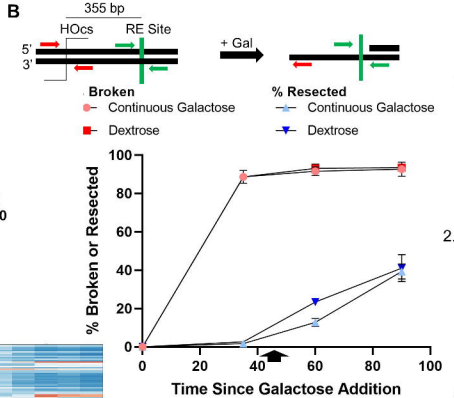
B
355 bp
HOcs
RE Site
5'
3'
+ Gal
Broken
Continuous Galactose
Dextrose
% Resected
Continuous Galactose
Dextrose
% Broken or Resected
Time Since Galactose Addition

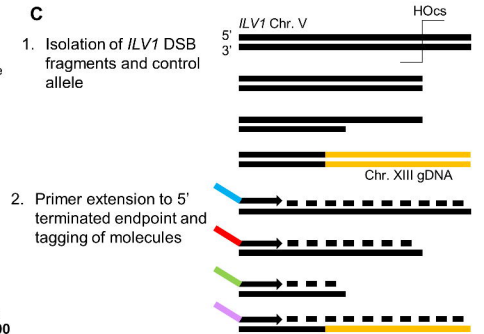
C
1. Isolation of ILV1 DSB fragments and control allele
ILV1 Chr. V
HOcs
5'
3'
Chr. XIII gDNA
2. Primer extension to 5' terminated endpoint and tagging of molecules
3. Intramolecular ligation and library amplification
P7
P5

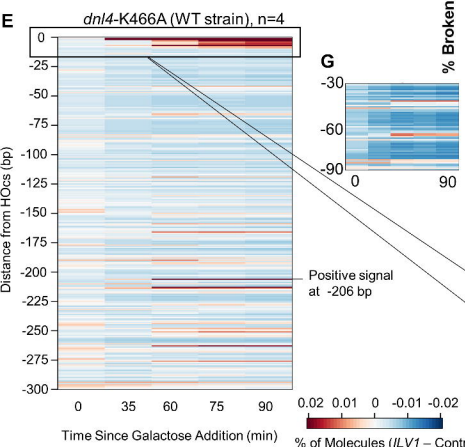
E
dnl4-K466A (WT strain), n=4
Distance from HOcs (bp)
Positive signal at -206 bp
Time Since Galactose Addition (min)
% of Molecules (ILV1 – Control)


G

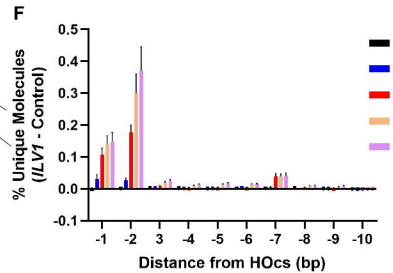
F
% Unique Molecules (ILV1 - Control)
T0
T35
T60
T75
T90
Distance from HOcs (bp)

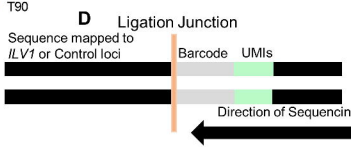
D
Ligation Junction
Sequence mapped to ILV1 or Control loci
Barcode
UMIs
Direction of Sequencing from P5

# Figure 2

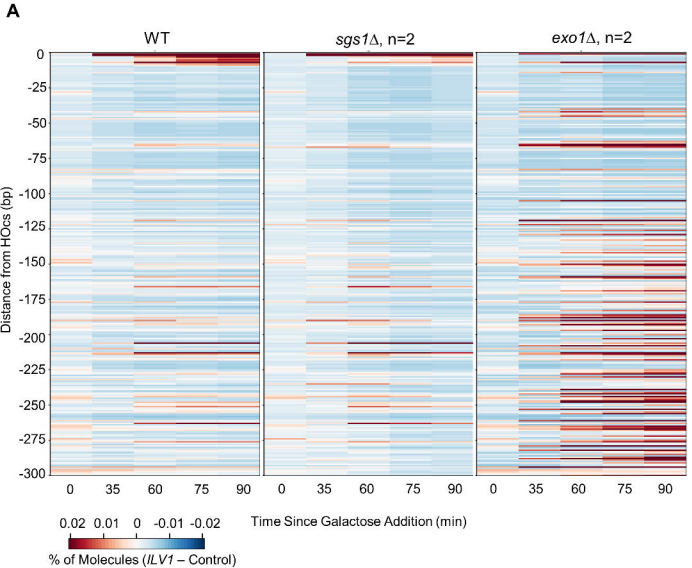
A
WT
sgs1Δ, n=2
exo1Δ, n=2
Distance from HOcs (bp)
0
-25
-50
-75
-100
-125
-150
-175
-200
-225
-250
-275
-300
0 35 60 75 90
Time Since Galactose Addition (min)
0.02 0.01 0 -0.01 -0.02
% of Molecules (ILV1 – Control)

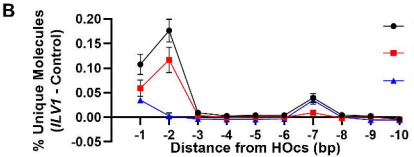
B
% Unique Molecules (ILV1 - Control)
0.20
0.15
0.10
0.05
0.00
-0.05
-1 -2 -3 -4 -5 -6 -7 -8 -9 -10
Distance from HOcs (bp)
T60 WT
T60 sgs1Δ
T60 exo1Δ

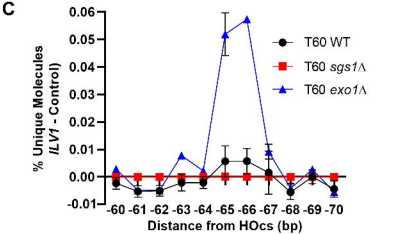
C
% Unique Molecules (ILV1 - Control)
0.06
0.05
0.04
0.03
0.02
0.01
0.00
-0.01
-60 -61 -62 -63 -64 -65 -66 -67 -68 -69 -70
Distance from HOcs (bp)
T60 WT
T60 sgs1Δ
T60 exo1Δ

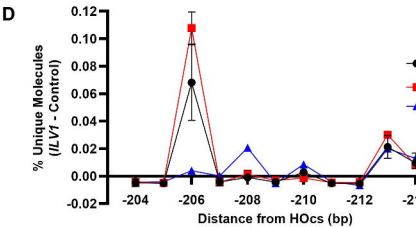
D
% Unique Molecules (ILV1 - Control)
0.12
0.10
0.08
0.06
0.04
0.02
0.00
-0.02
-204 -206 -208 -210 -212 -214
Distance from HOcs (bp)
T60 WT
T60 sgs1Δ
T60 exo1Δ

# Figure 3

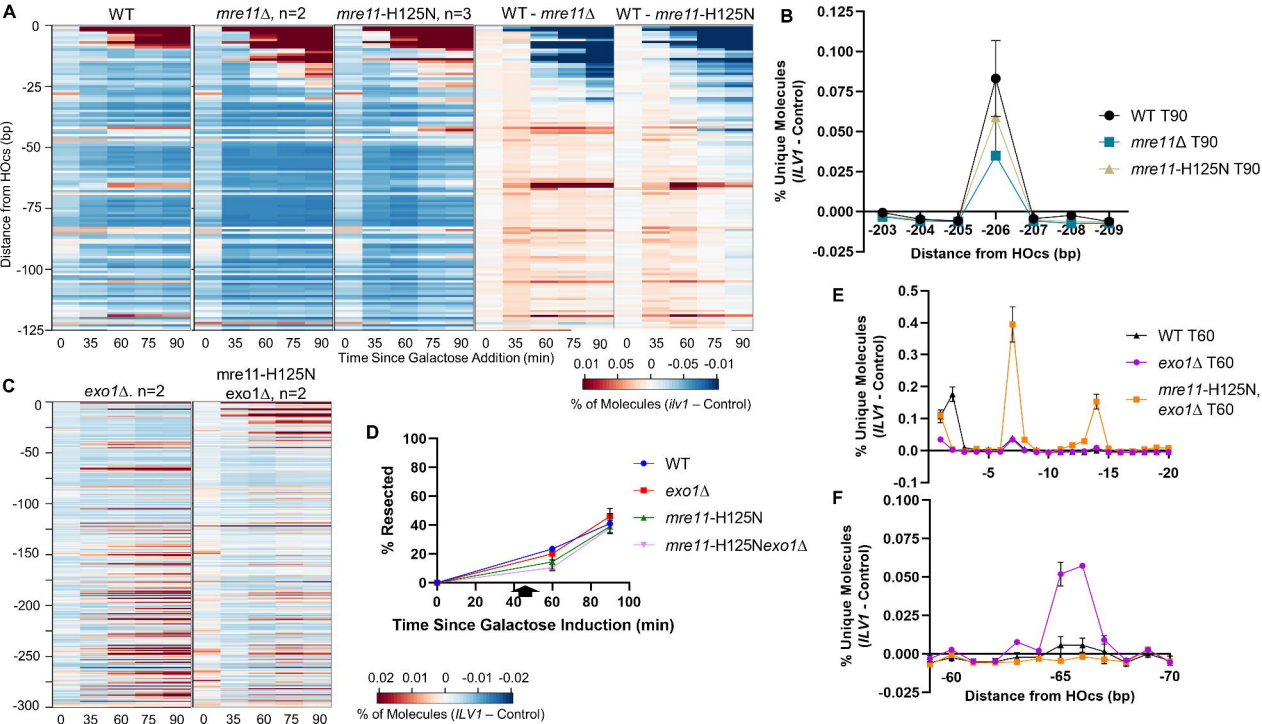
A
WT
mre11Δ, n=2
mre11-H125N, n=3
WT - mre11Δ
WT - mre11-H125N
Distance from HOcs (bp)
0
-25
-50
-75
-100
-125
0 35 60 75 90
Time Since Galactose Addition (min)
0.01 0.05 0 -0.05 -0.01
% of Molecules (ilv1 – Control)
B
% Unique Molecules (ILV1 - Control)
0.125
0.100
0.075
0.050
0.025
0.000
-0.025
-203 -204 -205 -206 -207 -208 -209
Distance from HOcs (bp)
WT T90
mre11Δ T90
mre11-H125N T90
C
exo1Δ. n=2
mre11-H125N exo1Δ, n=2
0
-50
-100
-150
-200
-250
-300
0 35 60 75 90
D
% Resected
100
80
60
40
20
0
0 20 40 60 80 100
Time Since Galactose Induction (min)
WT
exo1Δ
mre11-H125N
mre11-H125Nexo1Δ
0.02 0.01 0 -0.01 -0.02
% of Molecules (ILV1 – Control)
E
% Unique Molecules (ILV1 - Control)
0.5
0.4
0.3
0.2
0.1
0.0
-0.1
-5 -10 -15 -20
WT T60
exo1Δ T60
mre11-H125N, exo1Δ T60
F
% Unique Molecules (ILV1 - Control)
0.100
0.075
0.050
0.025
0.000
-0.025
-60 -65 -70
Distance from HOcs (bp)

# Figure 4

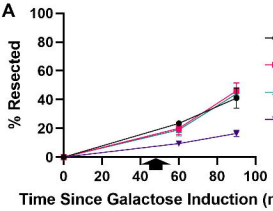
A
% Resected
Time Since Galactose Induction (min)
WT
exo1Δ
sgs1Δ
exo1Δsgs1Δ

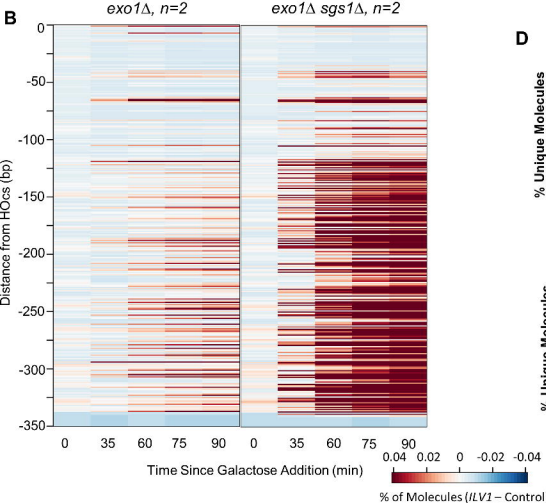
B
exo1Δ, n=2
exo1Δ sgs1Δ, n=2
Distance from HOcs (bp)
Time Since Galactose Addition (min)
% of Molecules (ILV1 – Control)

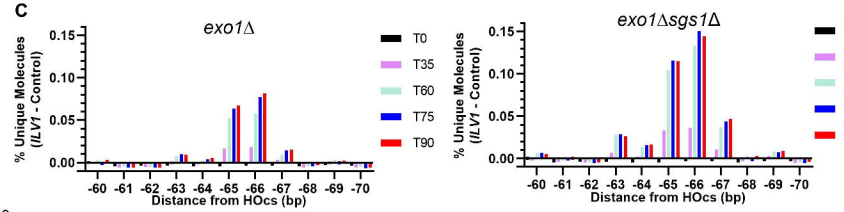
C
exo1Δ
exo1Δsgs1Δ
% Unique Molecules (ILV1 - Control)
Distance from HOcs (bp)
T0
T35
T60
T75
T90

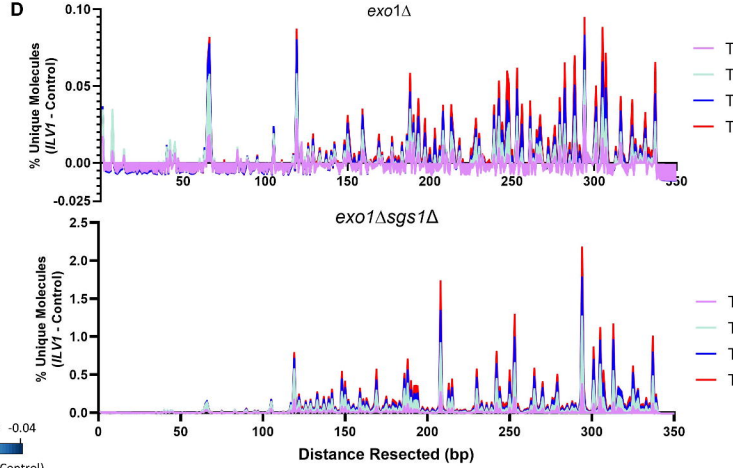
D
exo1Δ
exo1Δsgs1Δ
% Unique Molecules (ILV1 - Control)
Distance Resected (bp)
T35
T60
T75
T90

# Figure 5

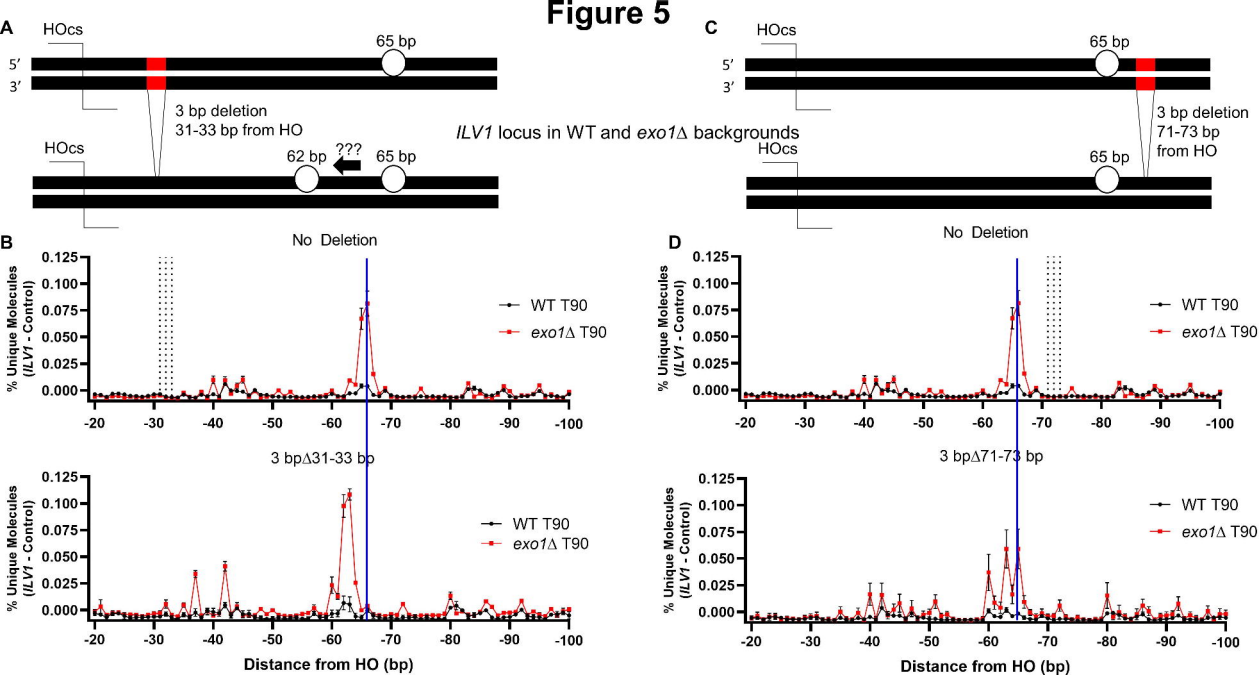
A
HOcs
65 bp
5′
3′
3 bp deletion
31-33 bp from HO
HOcs
62 bp
???
65 bp
ILV1 locus in WT and exo1Δ backgrounds
C
HOcs
65 bp
5′
3′
3 bp deletion
71-73 bp
from HO
HOcs
65 bp
B
No Deletion
% Unique Molecules
(ILV1 - Control)
0.125
0.100
0.075
0.050
0.025
0.000
-20
-30
-40
-50
-60
-70
-80
-90
-100
WT T90
exo1Δ T90
3 bpΔ31-33 bp
Distance from HO (bp)
D
No Deletion
3 bpΔ71-73 bp

# Figure 6

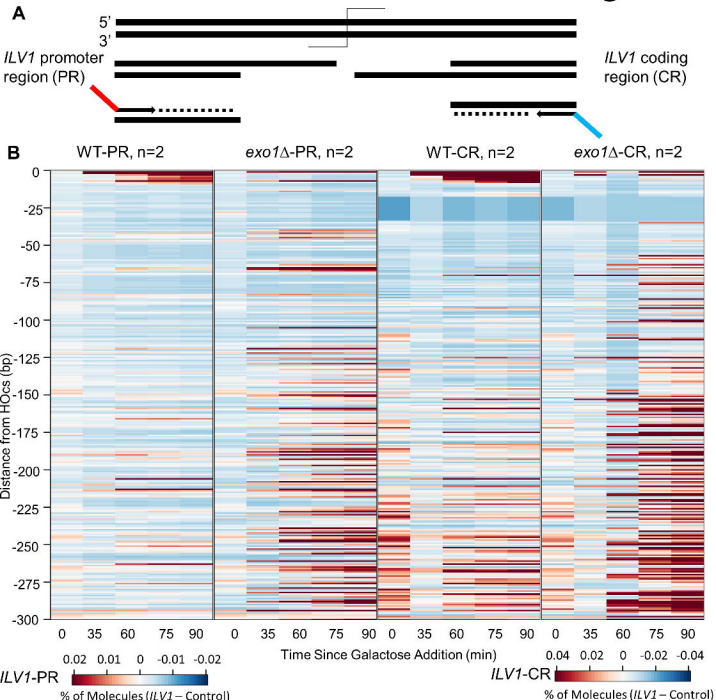
A
5'
3'
ILV1 promoter region (PR)
ILV1 coding region (CR)
B
WT-PR, n=2
exo1Δ-PR, n=2
WT-CR, n=2
exo1Δ-CR, n=2
Distance from HOcs (bp)
0
-25
-50
-75
-100
-125
-150
-175
-200
-225
-250
-275
-300
0 35 60 75 90
Time Since Galactose Addition (min)
ILV1-PR
0.02 0.01 0 -0.01 -0.02
% of Molecules (ILV1 – Control)
ILV1-CR
0.04 0.02 0 -0.02 -0.04
% of Molecules (ILV1 – Control)

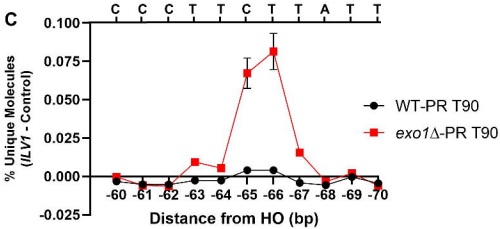
C
C C C T T C T T A T T
% Unique Molecules (ILV1 - Control)
0.100
0.075
0.050
0.025
0.000
-0.025
WT-PR T90
exo1Δ-PR T90
-60 -61 -62 -63 -64 -65 -66 -67 -68 -69 -70
Distance from HO (bp)

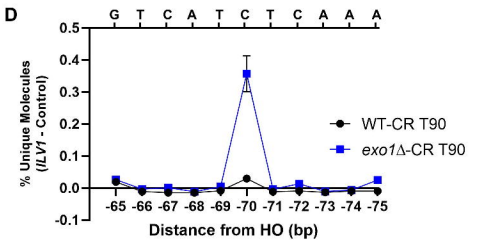
D
G T C A T C T C A A A
% Unique Molecules (ILV1 - Control)
0.5
0.4
0.3
0.2
0.1
0.0
-0.1
WT-CR T90
exo1Δ-CR T90
-65 -66 -67 -68 -69 -70 -71 -72 -73 -74 -75
Distance from HO (bp)

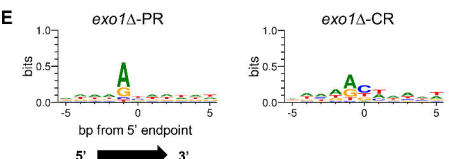
E
exo1Δ-PR
exo1Δ-CR
bits
1.0
0.5
0.0
-5
0
5
bp from 5' endpoint
5'
3'

# Figure 7

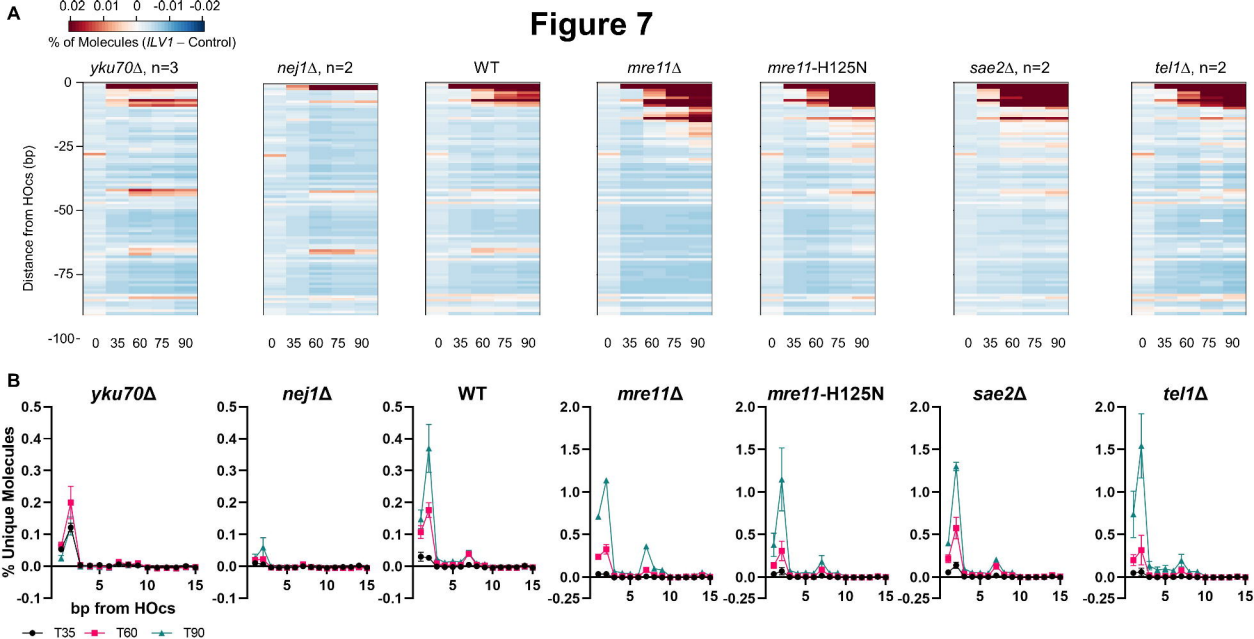
A
0.02 0.01 0 -0.01 -0.02
% of Molecules (ILV1 – Control)
yku70Δ, n=3
nej1Δ, n=2
WT
mre11Δ
mre11-H125N
sae2Δ, n=2
tel1Δ, n=2
Distance from HOcs (bp)
0
-25
-50
-75
-100
0 35 60 75 90
B
yku70Δ
nej1Δ
WT
mre11Δ
mre11-H125N
sae2Δ
tel1Δ
% Unique Molecules
bp from HOcs
T35
T60
T90